Backbone Dynamics of the c-Jun Leucine Zipper: ^{15}N NMR Relaxation Studies†

Joel P. Mackay,*,‡ Graeme L. Shaw,§ and Glenn F. King‡

Department of Biochemistry, University of Sydney, Sydney NSW 2006, Australia and Department of Biochemistry, University of Oxford, Oxford OX1 3QU, U.K.

Received November 21, 1995; Revised Manuscript Received February 5, 1996⊗

ABSTRACT: The backbone dynamics of the coiled-coil leucine zipper domain of c-Jun have been studied using proton-detected two-dimensional ^{1}H−^{15}N NMR spectroscopy. Longitudinal (T_1) and transverse (T_2) ^{15}N relaxation times, together with {^{1}H}^{15}N NOEs, were measured and analyzed by considering the protein to approximate a prolate ellipsoid. An analysis of the T_1/T_2 ratios for residues in the well-structured section of the protein showed that a model for the spectral density function in which the protein is considered to reorient anisotropically fitted the data significantly better than an isotropic model. Order parameters (S^2) in the range 0.7−0.9 were observed for most residues, with lower values near the C-terminus, consistent with fraying of the two helices comprising the coiled-coil. Because nearly all of the N−H vectors have small angles to the long axis of the molecule, there was some uncertainty in the value of the rotational diffusion coefficient D_{par}, which describes rotation about the long axis. Thus, an alternative method was examined for its ability to provide independent estimates of D_{par} and D_{perp} (the diffusion coefficient describing rotation about axes perpendicular to the long axis); the translational diffusion coefficient (D_t) of the protein was measured, and hydrodynamic calculations were used to predict D_{par} and D_{perp}. However, the derived rotational diffusion coefficients proved to be very dependent on the hydrodynamic model used to relate D_t to D_{par} and D_{perp}, and consequently the values obtained from the T_1/T_2 analysis were used in the order-parameter analysis. Although it has previously been reported that the side chain of a polar residue at the dimer interface, Asn22, undergoes a conformational exchange process and destabilizes the dimer, no evidence of increased backbone mobility in this region was detected, suggesting that this process is confined to the Asn side chain.

It has become clear in recent years that the highly specific molecular recognition processes which occur in biological systems are intimately dependent on the dynamic properties of the species concerned [see, for example, Bennett and Huber (1983), Karplus and McCammon (1983), Ringe and Petsko (1985), and Williams (1989)]. Such processes all comprise a delicate balance of enthalpic and entropic contributions (Page & Jencks, 1971; Jencks, 1981; Fersht, 1987; Williams *et al*., 1991), and an understanding of the nature of these motions will undoubtedly assist in, for example, the design of specific inhibitors of protein function.

The protein c-Jun is a eukaryotic transcriptional activator, deregulated expression of which has been implicated in the neoplastic transformation of cells (Angel & Herrlich, 1994). c-Jun is a member of the basic domain leucine zipper (bZIP) class of DNA-binding proteins; these proteins consist of two distinct domains, a highly basic DNA-binding domain and a leucine zipper domain (Landschulz *et al*., 1988). This leucine zipper domain mediates protein dimerization (both homodimerization and heterodimerization with other bZIP proteins), which juxtaposes the two DNA-binding domains so that they are able to bind their cognate enhancer sequence. These sequences all have dyad symmetry; each half of the dimer thus occupies one half-site on the DNA (Hurst, 1994). Protein dimerization is therefore a prerequisite for DNA binding, so the activity of these bZIP proteins is regulated not only by the interactions between the protein and DNA but equally by the protein−protein interactions between the leucine zipper domains (Alber, 1992).

Dimerization of leucine zipper proteins occurs via the formation of a parallel coiled-coil of α-helices. The leucine zipper is characterized by a heptad repeat of leucine residues (Landschulz *et al*., 1988), and, following conventional nomenclature for such repeats [(**abcdefg**)$_n$], the leucine residues are found at position **d** (Figure 1). Another heptad repeat of hydrophobic residues is found at position **a**, and together these **a**- and **d**-position residues form a hydrophobic dimer interface. It has been suggested that the coiled-coil is further stabilized by polar groups in the positions adjacent to the hydrophobic interface (**e** and **g**) forming interhelical ion-pairs (McLachlan & Stewart, 1975; Zhou *et al*., 1994), although the relative importance of electrostatic interactions in these dimers is presently unclear (Junius *et al*., 1996; Lumb & Kim, 1995). Note, however, that these polar residues contribute to the stability of the hydrophobic interface via the packing of their methylene groups against the residues in the **a** and **d** positions (O'Shea *et al*., 1991).

A notable feature of most bZIP proteins is a conserved **a**-position polar residue (usually Asn) at the hydrophobic interface (Hurst, 1994). X-ray crystallographic studies of the GCN4 leucine zipper (O'Shea *et al*., 1991) showed that this Asn residue adopts an asymmetric conformation in the otherwise generally symmetrical structure and that its side chain packs more loosely against adjacent residues than do other **a**-position side chains. Replacement of this Asn residue with a Val dramatically stabilizes the coiled-coil (Harbury

† This work was supported by a research grant to G.F.K. from the National Health and Medical Research Council of Australia. J.P.M. is supported by an Australian Research Council Postdoctoral Research Fellowship. G.L.S. thanks the Wellcome Trust for financial support.

* Address correspondence to this author.
‡ University of Sydney.
§ University of Oxford.

⊗ Abstract published in *Advance ACS Abstracts,* March 15, 1996.

0006-2960/96/0435-4867$12.00/0

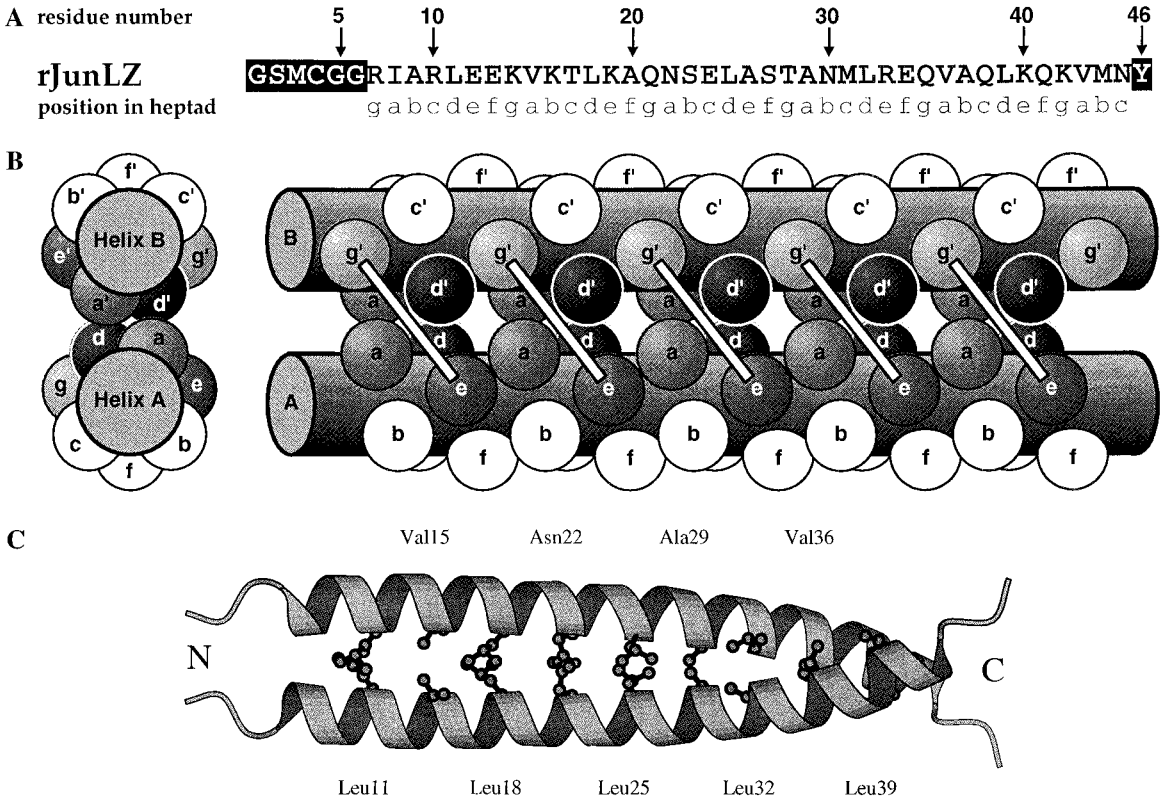

FIGURE 1: (A) Amino acid sequence of the rJunLZ monomer (Riley *et al*., 1994). The numbering for rJunLZ is shown, as well as the position of each residue in the heptad repeat. Non-native residues are indicated by reverse type. (B) Schematic representation of a parallel, two-stranded coiled-coil, with each residue denoted by a sphere. For simplicity, the supercoiling of the two helices is not shown. (C) Molscript (Kraulis, 1991) diagram of the sJunLZ homodimer (*i.e.*, rJunLZ without the residues Gly1, Ser2, and Met3), showing the **a**- and **d**-position residues at the dimer interface (Junius *et al*., 1996).

et al., 1993). We have recently shown that a similar situation exists for the homodimeric Jun leucine zipper (Junius *et al*., 1995), in which the homologous Asn (Asn22 in the recombinant peptide used in this study; Asn291 in native c-Jun) is involved in a conformational exchange process, thereby destabilizing the dimer in comparision to an Asn → Leu mutant. It has been suggested that the destabilization caused by this Asn residue may help to make dimerization reversible (O'Shea *et al*., 1991), thus facilitating the homo-/heterodimer exchange reactions crucial to the biological function of these transcription factors (Alber, 1992; McKnight, 1991).

Nuclear magnetic resonance (NMR) measurements of ^{15}N (and to a lesser extent, ^{13}C) nuclear spin relaxation times have been used widely in recent years to investigate the motions of individual atoms and domains within proteins on a time scale faster that the overall tumbling time of the molecule (Nirmala & Wagner, 1988, 1989; Kay *et al*., 1989; Palmer *et al*., 1991b). For example, Cheng *et al*. (1994) characterized changes in the backbone flexibility of FK506-binding protein following the binding of FK506, and Barbato *et al*. (1992) showed that the central linker region of calmodulin is very flexible in solution, in contrast to the ordered helical structure observed in the solid state by X-ray crystallography.

In this study, we have used ^{15}N relaxation measurements to probe the backbone dynamics of the homodimeric Jun leucine zipper, the solution structure of which we have recently solved (Junius *et al*., 1996). This work forms a part of our ongoing attempt to elucidate the balance of forces which determines specificity, affinity, and kinetics of leucine zipper formation. In particular we were interested in whether or not the destabilization of the native zipper by the interfacial Asn residue was manifested as an increase in backbone flexibility in that region of the coiled-coil. A method for providing an independent experimental estimate of the overall molecular tumbling time(s) is also examined: the translational diffusion coefficient of the c-Jun leucine zipper was measured using pulsed field gradient (PFG) NMR (Stejskal & Tanner, 1965; Kuchel & Chapman, 1991; Dingley *et al*., 1995) and used to derive estimates of the corresponding rotational correlation time(s).

MATERIALS AND METHODS

Materials. Sodium 3-(trimethylsilyl)[2,2,3,3-^{2}H]propionate (d_4-TSP) was obtained from Fluka AG (Buchs, Switzerland), while sodium azide and D_2O (99.99% isotopic purity) were purchased from Sigma Chemical Co. (St. Louis, MO). Human [98% U-^{15}N,^{13}C]ubiquitin was purchased from VLI Research (Wayne, PA). All other chemicals used were of analytical grade.

General. Production of recombinant c-Jun leucine zipper (rJunLZ) has been described previously (Riley *et al*., 1994). This peptide differs from a synthetic version used in our previous studies in that rJunLZ has three extra non-native residues at the N-terminus (46 residues in total, see Figure 1A). NMR experiments were performed on a sample containing 2.8 mg of uniformly ^{15}N-labeled rJunLZ dissolved in a solution composed of 450 μL of H_2O, 50 μL of D_2O, 5 μL of 10 mM d_4-TSP, and 5 μL of 100 mM NaN_3, pH 3.6. [U-^{13}C,^{15}N]Ubiquitin was prepared as a solution of 5 mg of protein in 450 μL of H_2O, 50 μL of D_2O, and 25 μM chloramphenicol, pH 4.0. All NMR measurements were carried out at 310 K on a Bruker AMX600 spectrometer,

except for the PFG diffusion measurements, which were performed at 298 K on a Bruker DRX500 equipped with an actively-shielded gradient probe. The magnitude of the pulsed field gradients has been shown to be linear over a length of 20 mm; the samples used for diffusion measurements were therefore prepared in 5-mm susceptibility-matched microcells (Shigemi, Japan), so the depth of the sample did not exceed 18 mm.

^{15}N Relaxation Theory. The relaxation of ^{15}N magnetization is dependent primarily on the dipolar interaction with its attached proton(s) and on its chemical shift anisotropy. Equations describing T_1, T_2, and the $\{^1H\}^{15}N$ NOE in terms of spectral density functions have been given previously (Abragam, 1961; Stone *et al*., 1992). These equations require a value for the N−H bond length which was assumed to be 1.02 Å in this work. The magnitude of the ^{15}N chemical shift anisotropy ($\sigma_{par} - \sigma_{perp}$) has been shown to be dependent on the conformation of the polypeptide chain (Shoji *et al*., 1989, 1990); since rJunLZ is helical, a value of −160 ppm was used in our calculations.

The spectral density, $J(\omega_i)$, depends on both the overall motion of the protein and the local motions occurring within the protein. The most common approach toward extracting motional parameters from ^{15}N relaxation measurements uses the model-free formalism of Lipari and Szabo (1982a,b). Lipari and Szabo showed that when the overall motion is isotropic and the internal motions are much faster than the rate of overall tumbling, a good model for the spectral density function is

$$J(\omega_i) = {}^2/_5\left[\frac{S^2\tau_M}{1+(\omega_i\tau_M)^2} + \frac{(1-S^2)\tau}{1+(\omega_i\tau)^2}\right] \quad (1)$$

where τ_M is the correlation time for overall tumbling of the protein. The order parameter, S^2 ($0 \le S^2 \le 1$), describes the extent of restriction of local motions at individual ^{15}N nuclei, and $1/\tau = 1/\tau_M + 1/\tau_e$, where τ_e is the (residue-specific) effective correlation time for the local motions.

This model only applies to proteins that tumble isotropically in solution. For a protein which tumbles anisotropically, it is not strictly valid to treat the overall motion and the internal motions separately. If, however, the internal motions occur on a time scale that is much faster than the rate of overall tumbling, then treating the two types of motions independently is a reasonable approximation (Lipari & Szabo, 1982b). In this case, for an axially symmetric molecule with different rotational diffusion coefficients parallel (D_{par}) and perpendicular (D_{perp}) to the unique axis of the molecule, the spectral density function may be written as (Woessner, 1962; Huntress, 1968; Zheng *et al*., 1995)

$$J(\omega_i) = {}^2/_5S^2\left[\frac{A_1\tau_1}{1+(\omega_i\tau_1)^2} + \frac{A_2\tau_2}{1+(\omega_i\tau_2)^2} + \frac{A_3\tau_3}{1+(\omega_i\tau_3)^2}\right] + {}^2/_5(1-S^2)\left[\frac{A_1\tau_1'}{1+(\omega_i\tau_1')^2} + \frac{A_2\tau_2'}{1+(\omega_i\tau_2')^2} + \frac{A_3\tau_3'}{1+(\omega_i\tau_3')^2}\right] \quad (2)$$

where

$$A_1 = 0.75\sin^4\alpha \quad (3)$$

$$A_2 = 3\sin^2\alpha\cos^2\alpha \quad (4)$$

$$A_3 = (1.5\cos^2\alpha - 0.5)^2 \quad (5)$$

and α is the angle between the N−H vector and the unique axis of the molecule. τ_i' is given by $1/\tau_i' = 1/\tau_i + 1/\tau_e$, where τ_i ($i = 1$, 2, or 3) are overall correlation times for the protein, given as combinations of the two rotational diffusion coefficients:

$$\tau_1 = (2D_{perp} + 4D_{par})^{-1} \quad (6)$$

$$\tau_2 = (5D_{perp} + D_{par})^{-1} \quad (7)$$

$$\tau_3 = (6D_{perp})^{-1} \quad (8)$$

The residue-specific parameters A_1, A_2, and A_3 may be determined from the coordinates of the three-dimensional structure of the protein (see below). Thus, there are four parameters remaining to be determined: the two global rotational diffusion coefficients (D_{perp} and D_{par}), the order parameter S^2, and the effective correlation time for internal motions, τ_e.

^{15}N Relaxation Experiments. The pulse sequences used for the measurement of T_1 and T_2, together with one of the experiments used to measure the NOE, are essentially those used by Kördel *et al.* (1992). These spectra were recorded using the sensitivity-enhancement procedure developed by Palmer *et al.* (1991a,b), which allows two orthogonal components of the magnetization to be recorded simultaneously, giving two independent pure-phase data sets after suitable deconvolution. Such data sets may be added together to yield a theoretical improvement in signal-to-noise of $\sqrt{2}$ over a conventional spectrum recorded in the same total time; in this case, however, the two data sets were not co-added but instead used as independent duplicates. Thus, two estimates of T_1, T_2, and the NOE may be obtained in the same time as a single conventional experiment.

Transverse relaxation times were measured by monitoring the peak height as a function of the length of an ^{15}N spin-locking pulse. Thus, in principle, the measured relaxation times, $T_{1\rho}$, differ from T_2 since $T_{1\rho}$ is dependent on the angle between the axis of the spin-locking pulse and the axis of the effective field. In this work the rf field strength of the spin-locking pulse was 2.9 kHz which locks the magnetization about an axis within ±9° of the transverse plane. Under these circumstances, and in the absence of low-frequency perturbations, $T_{1\rho}$ should be equivalent to T_2, allowing the distinction between the two to be dropped. During the variable delay of the T_1 experiment, τ, and the spin-locking pulse of the T_2 experiment, τ, synchronous proton decoupling was applied using the GARP-1 sequence (Shaka *et al*., 1985) to remove the effects of cross-correlation between dipolar and chemical shift anisotropy (CSA) relaxation mechanisms from the data (Boyd *et al*., 1990). The T_1 spectra were recorded with τ delays of 50, 150, 350, 600, 1000, 1500, 2000, 2500, and 3500 ms, while the T_2 measurements used values of 10, 30, 60, 100, 150, 250, 500, 750, and 1000 ms. Measurement of the $\{^1H\}^{15}N$ NOE requires the acquisition of two experiments, one with ^{1}H decoupling applied during the recycle delay and one without. The NOE was measured using two different pule sequences; the reason for this is discussed in the Results. In the first experiment (Kördel *et al*., 1992), water suppression was achieved using a purge pulse, while in the second experiment all proton pulses are

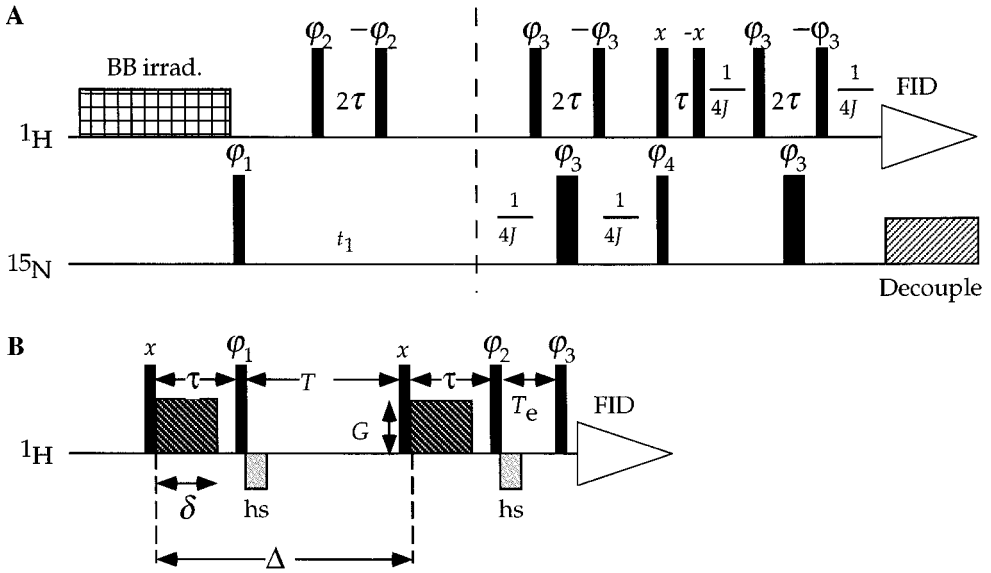

FIGURE 2: Pulse sequences for the measurement of (A) the $\{^1H\}^{15}N$ NOE, using $1-\bar{1}$ pulses for water suppression (Sørensen *et al*., 1995) and (B) the translational diffusion coefficients of rJunLZ and ubiquitin (Gibbs & Johnson, 1991; Waldeck *et al*., 1993). In A, the phase cycling was $\varphi_1 = (x, -x)$; $\varphi_2 = (x, -x, y, -y)$; $\varphi_3 = 16(x, -x)$; $\varphi_4 = 2(y, -y)$; acq = $(x, -x, -x, x)$. The broadband ^{1}H irradiation used to generate the NOE consisted of a WALTZ-16 broadband decoupling sequence. Quadrature detection was achieved using TPPI on φ_1. In B, the phase cycling was $\varphi_1 = (x, -x)$; $\varphi_2 = 2(x)$, $2(-x)$; $\varphi_3 = 4(x)$, $4(y)$, $4(-x)$, $4(-y)$; acq = $(x, -x, -x, x, y, -y, -y, y, -x, x, x, -x, -y, y, y, -y)$. Negative homospoil gradient pulses (hs) were used to eliminate any transverse magnetization remaining at the beginning of the longitudinal storage periods. The magnetic field gradients used for diffusion labeling were applied for time δ with an amplitude of G G cm^{-1}. The time period τ was kept constant to eliminate any contribution to signal decay from T_2 relaxation and J modulation (Dingley *et al*., 1995). Δ is the total time allowed for molecular diffusion, and T_e is a delay to allow for the dissipation of eddy-current effects arising from the field gradients prior to acquisition.

replaced with $1\text{-}\bar{1}$ (jump−return, JR) pulses (Figure 2A; Sørensen *et al*., 1995).

All spectra were recorded with spectral widths of 802 and 5747 Hz in F_1 and F_2, respectively, using acquisition times of 79 and 356 ms in t_1 and t_2, respectively. The carrier frequency was set to the frequency of the water resonance in F_2 and to the center of the ^{15}N spectrum in F_1. The amide proton resonances of Gly5 and Gly6 were folded in the ^{15}N dimension in order to increase spectral resolution in F_1 (see Figure 3). INEPT delays were set to 2.8 ms. Water suppression was achieved using a pair of orthogonal purge pulses (Messerle *et al*., 1989) in the T_1 and T_2 experiments, together with very weak selective irradiation of the water resonance during part of the recycle delay. For the sensitivity-enhanced NOE experiment, a single purge pulse was applied immediately prior to the first ^{15}N pulse. In all cases, a post-acquisition filter was applied to reduce further the intensity of the water resonance (Marion *et al*., 1989). Quadrature detection was achieved in t_1 using time-proportional phase incrementation (TPPI; Marion & Wüthrich, 1983). The total recycle delay between transients was set to 4.2 s for the T_1 and T_2 experiments and to 12 s for the NOE experiments, although experiments were recorded with shorter recycle delays for comparison. The number of scans per t_1 increment was 32 for the T_1 and T_2 experiments and 32−64 for the NOE experiment. The JR NOE experiment was carried out twice with the JR delay tuned to give different intensity maxima (130 and 103 μs gave maxima at 7.9 and 8.7 ppm, respectively), as the bandwidth over which reasonable sensitivity is obtained in this experiment is rather narrow (Sørensen *et al*., 1995). These two experiments were both duplicated to provide an error estimate for data recorded at each offset; weighted means were calculated subsequently from each pair of measurements. This procedure takes into account the offset dependence of the signal intensities in the JR NOE experiment.

PFG Diffusion Experiments. Translational diffusion coefficients for both rJunLZ and ubiquitin were determined using the PFG longitudinal eddy-current delay (LED) pulse sequence (Figure 2B; Gibbs & Johnson, 1991; Waldeck *et al*., 1993). Each diffusion measurement was obtained from a series of twelve PFGLED spectra in which the delay periods τ (20 ms), Δ (50 ms), and T_e (4 ms) and the magnitude of the gradients (G, 11.0 G cm^{-1}) were held constant, and the length of the field gradient pulses was incremented in 1.75-ms steps (from 0 to 19.25 ms in the final spectrum). A "dummy" experiment (G = 0 G cm^{-1}) was acquired at the beginning of each series to ensure the sample had reached thermal equilibrium.

Data Processing. Data were processed on a Silicon Graphics Indigo R4000 computer, using a combination of commercial software (UXNMR) and programs written in-house. The ^{1}H-frequency scale of all spectra was directly referenced to TSP at 0.00 ppm, while the ^{15}N-frequency scale was indirectly referenced to liquid NH_3 via the ^{1}H frequency of the TSP resonance (Live *et al*., 1984). Cross-peaks in the ^{1}H−^{15}N correlation spectra were well-resolved, except for a small amount of overlap observed between the signals from residues Ala9, Leu11, Gln35, and Met44 (see Figure 3). Linear prediction was used in t_1 to extend the data from 128 real points to 192 real points. The data were zero-filled once in each dimension, multiplied by weighting functions (Lorentz−Gauss function in t_2 and a squared shifted-sine-bell in t_1), and then transformed to give final data matrices of 2048 (F_2) × 128 (F_1) real points. Polynomial base line corrections were applied to the processed spectra in F_2.

All diffusion experiments were recorded using 8192 complex data points and a spectral width of 6000 Hz. Free induction decays were multiplied by a decaying exponential function with a decay constant of 2 Hz before Fourier transformation.

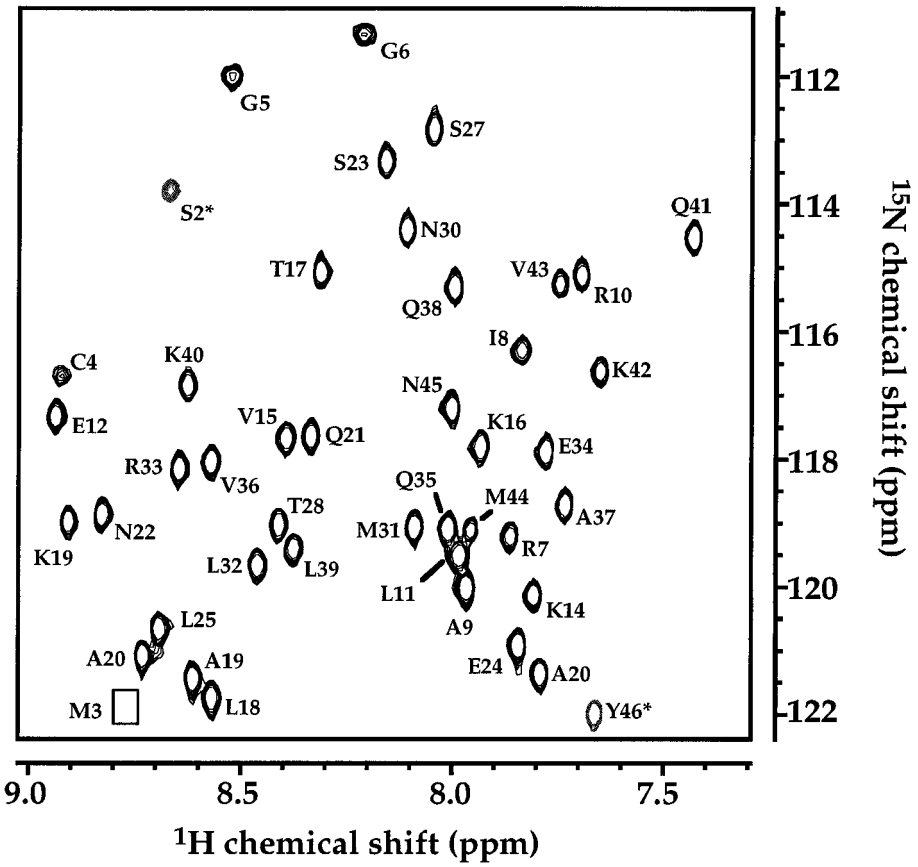

FIGURE 3: Example of a sensitivity-enhanced $\{^1H\}^{15}N$ NOE spectrum of rJunLZ. The signals from Gly5 and Gly6 are aliased in the F_1 dimension. Ser2 and Tyr46 have negative cross-peak intensities (marked with an asterisk) due to their large, negative NOEs, and Met3 shows zero intensity due to its NOE of −1. It can be seen that there is very little overlap which could adversely affect measured peak intensities in the relaxation experiments. The resonance of Gly1 cannot be detected under the experimental conditions.

Calculation of Relaxation Rates and NOEs. Cross-peak heights were measured using the program XEASY (Bartels *et al*., 1995), which was kindly provided by Professor K. Wüthrich. T_1 values were calculated for each residue from three-parameter nonlinear fits of the experimental data to eq 9:

$$I(\tau) = I_\infty - [I_\infty - I_0]\exp(-\tau/T_1) \quad (9)$$

T_2 values were likewise obtained from three-parameter fits to the equation

$$I(\tau) = I_\infty + I_0 \exp(-\tau/T_2) \quad (10)$$

In these equations I_0 and I_∞ are the cross-peak intensities at zero- and infinite-time, respectively. Nonlinear least-squares curve-fitting was carried out using the program KaleidaGraph 3.0 (Synergy Software, Reading, PA). Uncertainties in the fitted relaxation times were taken to be the standard errors given by the program. T_1 and T_2 values were calculated for each duplicate dataset separately, and from these, weighted average means/grouped SDs were then derived. Note that rms base line noise levels were not used to estimate the error in peak heights, as we found that this would have led to significantly underestimated errors. A similar observation was made recently by Skelton *et al*. (1993). The $\{^1H\}^{15}N$ NOEs were calculated as fractional enhancements according to eq 11

$$f_1\{S\} = (I_{sat} - I_{ref})/I_{ref} \quad (11)$$

where I_{sat} and I_{ref} are the cross-peak intensities in the presence and absence of ^1H saturation, respectively. The sensitivity-enhanced NOE experiment was repeated four times (see Results), and the peak heights from the resulting eight datasets were averaged to yield error estimates of the peak heights. For the JR NOE experiment, a similar method was used to calculate the NOEs.

Analysis of ^{15}N Relaxation Data. The T_1/T_2 ratios were fitted to different models describing the tumbling of rJunLZ, in order to determine which model best describes the molecule. The models for overall motion were fitted to the T_1/T_2 data by minimizing the error function

$$\chi^2 = \sum_i \left[\frac{(T_1/T_2)_{calc,i} - (T_1/T_2)_{obs,i}}{\sigma_{obs,i}}\right]^2 \quad (12)$$

where $(T_1/T_2)_{obs,i}$ and $(T_1/T_2)_{calc,i}$ are the observed and calculated values of the T_1/T_2 ratio, respectively, and $\sigma_{obs,i}$ is the error in $(T_1/T_2)_{obs,i}$. The sum is carried out over the residues that are found in "well-structured" regions of the protein (see below). To calculate χ^2 using an anisotropic tumbling model, the angle between each N−H vector and the unique axis of the ellipsoid, α_i, must be known. These angles were calculated from the atomic coordinates of the seven best solution structures of rJunLZ (Brookhaven Protein Data Bank, 1jun; Junius *et al*., 1996) using the following procedure. The coordinates were first used to calculate the inertial tensor for the molecule; this tensor was subsequently diagonalized. Since the eigenvector of the smallest eigenvalue of inertial tensor corresponds to the long axis of the molecule, the angle between each N−H vector and this axis

can be calculated from the dot product of the two vectors. This procedure was repeated for each solution structure, giving a number of estimates for α_i. These estimates were then averaged, and the uncertainty in α_i was taken from the standard deviation. Each estimate of α_i actually comprised an average of two symmetrically related residues since rJunLZ is a symmetric dimer.

Residues *i* were excluded from the T_1/T_2 fit (Barbato *et al*., 1992) when both

$$\text{(a) } \mathrm{NOE}_i < -0.35 \tag{13a}$$

and

$$\text{(b) } T_{2,i} < \langle T_2 \rangle - \sigma_{T_2} \quad \text{and} \quad \frac{(T_{2,i} - \langle T_2 \rangle)}{T_{2,i}} > \frac{3(\langle T_1 \rangle - T_{1,i})}{T_{1,i}} \tag{13b}$$

where $\langle T_1 \rangle$ and $\langle T_2 \rangle$ are the mean T_1 and T_2 values taken over all residues and σ_{T_2} is the standard deviation of the T_2 data.

The goodness of fit of the various models for rJunLZ tumbling was assessed using an *F* statistic. To compare χ^2 from two models with ν_1 and ν_2 degrees of freedom ($\nu_1 > \nu_2$), the *F*-test statistic is

$$F(\nu_1,\nu_2) = \nu_2\left(\frac{\chi^2(\nu_1) - \chi^2(\nu_2)}{\chi^2(\nu_2)}\right) \tag{14}$$

where $\chi^2(\nu_i)$ is the value of χ^2 for the model with ν_i degrees of freedom. A small *F* statistic indicates that there is no difference between the ability of the two models to explain the data, and a large *F* statistic indicates that the more complex model is justified.

Calculation of Translational Diffusion Coefficients. The signal intensity (R_t) recorded in a PFG diffusion experiment is given by

$$R_t = R_\infty + R_0 \exp\{-\gamma^2 G^2 D \delta^2 (\Delta - {}^{\delta}/_{3})\} \tag{15}$$

where *G* and δ are the strength and duration of the gradient pulses, respectively, Δ is the time between gradient pulses, γ is the magnetogyric ratio of the observed nucleus, and R_∞ and R_0 are the normalized resonance intensities at infinite- and zero-time, respectively. A nonlinear least-squares fit of the PFG data yields the translational diffusion coefficient and an estimate of its error. For both rJunLZ and ubiquitin, several resonances were used to determine diffusion coefficients and weighted means were calculated.

The molecular masses (*M*) of both ubiquitin and rJunLZ were estimated from their measured diffusion coefficients (D_t), using the equation (Cantor & Schimmel, 1980; Dingley *et al*., 1995)

$$M = \left(\frac{kT}{6\pi\eta F D_t}\right)^3 \left(\frac{4\pi N_a}{3[\bar{\nu}_2 + \delta\bar{\nu}_1]}\right) \tag{16}$$

where η is the viscosity of the solvent, *F* is the Perrin factor which relates to molecular shape [see Cantor and Schimmel (1980) and Dingley *et al*. (1995)], N_a is Avogadro's number, $\bar{\nu}_2$ is the partial specific volume of the protein, δ_1 is the fractional amount of water bound to the protein (typically, 0.3−0.4 g of H_2O per g of protein), and $\bar{\nu}_1$ is the partial specific volume of the solvent.

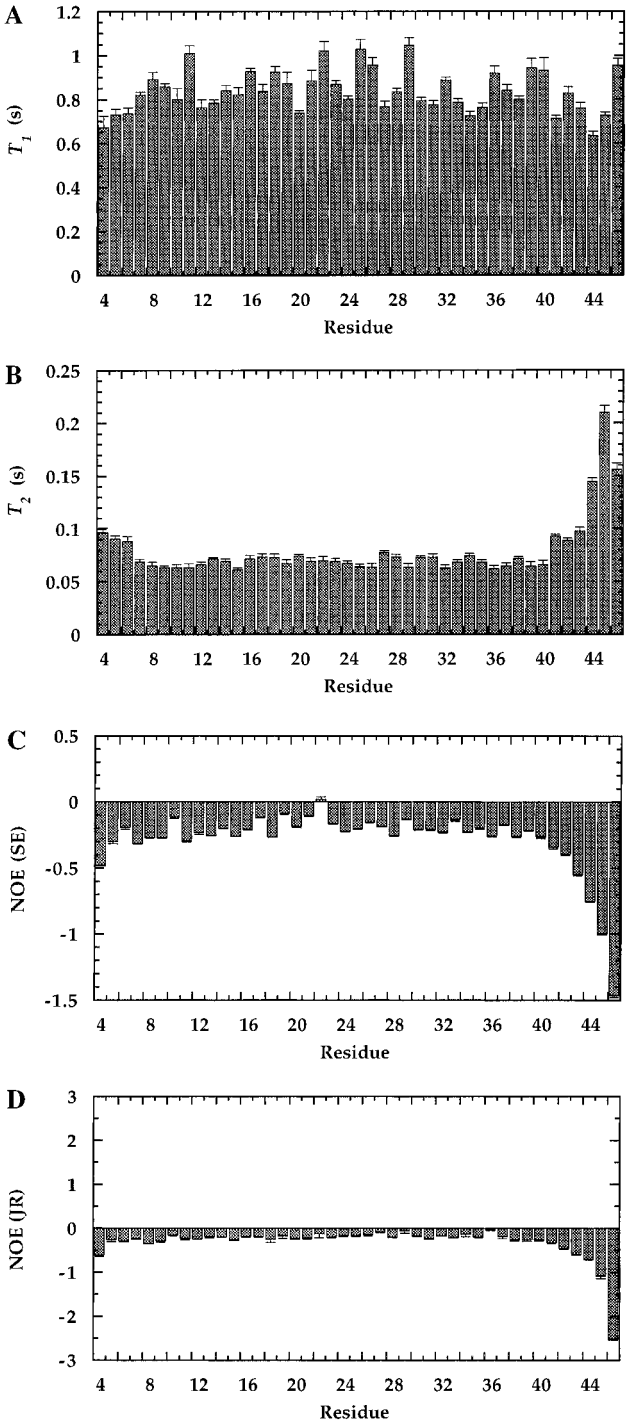

FIGURE 4: Derived values of (A) T_1, (B) T_2, and (C, D) $\{^1H\}^{15}N$ NOE for the rJunLZ dimer. The uncertainties are plotted as standard errors. C shows the NOEs derived from the sensitivity-enhanced NOE experiment, while D shows the NOEs derived from the JR NOE experiment. Note that values for residues Ser2 and Met3 are not given (see text).

RESULTS AND RELAXATION ANALYSIS

Determination of the Model for Overall Motion. Figure 4 shows the derived T_1, T_2, and NOE values; NOE data determined from both the sensitivity-enhanced and JR NOE experiments are shown for comparison. The average standard errors were 3.3% (T_1), 4.0% (T_2), 5.6% (sensitivity-enhanced NOE), and 16% (JR NOE). Although the errors were significantly larger for the JR NOE experiment

compared with the sensitivity-enhanced NOE experiment, we chose to combine the data from both experiments for the model-free analysis. For two residues, the $\{^1H\}^{15}N$ NOE is more positive than the maximum value predicted from theory; this has been observed in other studies [*e.g.*, Rischel *et al*. (1994)]. In particular, this was noted for Asn22 when the NOE was measured using the sensitivity-enhanced pulse sequence. It is possible for the combination of chemical exchange between the amide proton and solvent water, and the slow longitudinal relaxation of the water magnetization, to lead to erroneously high NOE measurements (Grzesiek & Bax, 1993). If saturation of the water magnetization is minimized, then this problem can be reduced; one way of achieving this aim is to use the JR NOE sequence (Figure 2A). The use of this sequence reduced the size of the positive NOE measured for Asn22; however, it still remained larger than expected from theory.

The first step in the analysis of the relaxation data is to determine whether the shape of the protein may be best approximated by a sphere or by a symmetric ellipsoid so that either eq 1 or eq 2 may be chosen to analyze the data. In the case of rJunLZ, visual inspection of the three-dimensional structure suggests that the overall motion of the protein should be modeled using a prolate ellipsoid. This can be confirmed by calculating the axial ratio of the inertial tensor; in the case of rJunLZ the axial ratio of the inertial tensor is 2.78:2.75:1 (see below). Although both visual inspection and the use of the inertial tensor suggest that an ellipsoidal model for overall motion should be used, a more quantitative approach to choosing the model is preferable. This can be achieved by fitting the T_1/T_2 ratio using the different models; the model which gives the best fit to the data is deemed the most suitable (Zheng *et al*., 1995). The T_1/T_2 ratio is used in this procedure since, in the absence of slow internal motions ($\tau_e < 100$ ps, $S^2 > 0.7$), the T_1/T_2 ratio is independent of both S^2 and τ_e (Kay *et al*., 1989; Clore *et al*., 1990) and depends only on the parameters describing overall motion. The error function described in Materials and Methods (eq 12) was minimized, with the summation including only the residues which are found in well-structured regions of the protein (see below). Since the solution structure was calculated using constraints derived largely from a synthetic peptide, which lacked residues Gly1, Ser2, and Met3 of rJunLZ, angles could not be derived for these residues, and they were excluded from these, and all further, calculations. 3D NOESY-HMQC data (Junius *et al*., 1995), together with the raw ^{15}N relaxation data, suggest that these residues are highly mobile and probably completely unstructured. In addition, other residues were excluded using the criteria described in Materials and Methods (eqs 13a and 13b). On this basis, Cys4 and the C-terminal residues Lys42−Tyr46 were excluded from the T_1/T_2 calculations.

The models for the overall motion tested in this way included (i) an isotropic overall tumbling model; (ii) an anisotropic ellipsoidal tumbling model with the ratio of D_{par} to D_{perp} fixed to 2.77:1 (from the inertial tensor calculation); (iii) an anisotropic ellipsoidal tumbling model with both D_{par} and D_{perp} varied freely. Table 1 shows χ^2, the fitted parameters, and the degrees of freedom for each model. This analysis indicates that model iii achieves the best fit to the T_1/T_2 data, but it does not indicate whether the improvement in the fit justifies the increased complexity of model iii. One criterion which can be used to answer this question is the statistical F test (eq 14). Comparing model iii with models i and ii gives relatively large F statistics of 14.9 and 6.2, respectively. The probabilities that these statistics could have arisen simply by chance are 7×10^{-13} and 2×10^{-7}, respectively, indicating that model iii explains the data better than either model i or ii.

Table 1: Determination of the Most Appropriate Model for Overall Motion of the rJunLZ Dimer[a]

model	parameters	degrees of freedom	χ^2	fitted parameters ($\times 10^{-7}$ s^{-1})
i	D_{iso}	36	577.2	$D_{iso} = 1.69$
ii	D_{perp}, D_{par} (fixed ratio)	36	476.7	$D_{par} = 2.77 \times D_{perp} = 4.04$
iii	D_{perp}, D_{par}	35	405.1	$D_{par} = 2.80$; $D_{perp} = 1.56$

[a] As outlined in the text, χ^2 in eq 12 was minimized over all residues for different models of overall tumbling. Model i assumes isotropic reorientation in solution. Model ii allows for anisotropic tumbling (with axial symmetry) but fixes the ratio of D_{par}/D_{perp} from the inertial tensor calculation. Model iii allows both D_{par} and D_{perp} to vary freely in the minimization.

However, if model iii is to be used to analyze the relaxation data, then it is important to assess the precision of the rotational diffusion coefficients, in particular D_{par}, since the majority of the residues used in the calculation have N−H angles of less than *ca.* 30° to the long axis of the molecule. As a consequence, rotational diffusion about the long axis has less effect on the ^{15}N relaxation parameters than rotation about the two short axes. In addition, there is some uncertainty in the angle between each N−H vector and the principal axis of the protein; this uncertainty may be carried through to the estimates for the rotational diffusion coefficients. To determine the uncertainty in the rotational diffusion coefficients, 500 Monte Carlo simulations were performed which took into account both the uncertainty in the T_1/T_2 ratio and the uncertainty in α_1. The diffusion coefficients were determined as $D_{par} = (2.8 \pm 0.5) \times 10^7$ m^2 s^{-1} and $D_{perp} = (1.56 \pm 0.05) \times 10^7$ m^2 s^{-1} (using model iii above), where the uncertainties are the standard deviations from the Monte Carlo simulations. These results indicate that the estimates of the rotational diffusion coefficients are precise enough to use as initial estimates but that further refinement would be desirable.

Because of the uncertainty in the estimate for D_{par} we decided to try to obtain independent estimates of the magnitudes of D_{par} and D_{perp}. The simplest approach would be to calculate the rotational diffusion coefficients directly using standard hydrodynamic equations (Cantor & Schimmel, 1980). However, the reliability of this approach can suffer as a result of the approximations on which it is based; most notably, that the protein can be adequately modeled as a sphere or axially symmetric ellipsoid with a smooth surface. A more accurate approximation involves modeling the protein as a collection of spheres (point sources of friction) in a solvent continuum and calculating directly the elements of the rotational (and translational) diffusion tensor for that model (Torre & Bloomfield, 1981, 1989). The atomic coordinates of the protein (taken from either an NMR- or X-ray-derived structure) can be used to define the positions of the spheres—a useful approach is to use only C^α atoms and to represent them as spheres with radius 3.5 Å. However, such models generally predict translational diffusion coefficients that are larger than experimentally observed values. The explicit inclusion of an partial layer of water can be used to correct for this difference, although it is

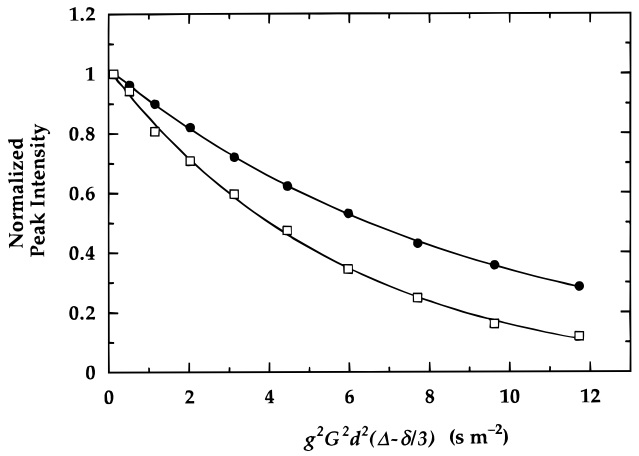

FIGURE 5: Peak intensities, from ^{1}H PFGLED NMR experiments, for representative signals from rJunLZ (●) and ubiquitin (O), plotted as a function of $\gamma^2G^2\delta^2(\Delta - \delta/3)$. Nonlinear regression of eq 15 onto the data (solid line) yielded the translational diffusion coefficients.

Table 2: Predicted Translational and Rotational Diffusion Coefficients for Ubiquitin from the Hydrodynamics Programs HYDRO and HI4 Together with the Experimentally Determined Translational Diffusion Coefficient[a]

	D_t ($\times 10^{10}$ m^2 s^{-1})	D_{xx} ($\times 10^{-7}$ s^{-1})	D_{yy} ($\times 10^{-7}$ s^{-1})	D_{zz} ($\times 10^{-7}$ s^{-1})
HYDRO[b]	1.69	2.57	2.63	3.18
HI4[c]	1.77	5.35	6.07	9.47
HYDRO + H_2O[b,d]	1.47	1.98	2.01	2.40
D_t (obs)[d]	1.52			

[a] All calculations were carried out using the C^α atom coordinates from the Brookhaven Protein Data Bank file 1ubq, so that the protein is represented as 76 spheres with 3.5 Å radii (T = 298 K, η = 8.904 $\times 10^{-4}$ kg m^{-1} s^{-1}). Note that D_{zz} corresponds to D_{par} and that $D_{xx} \approx D_{yy}$ corresponds to D_{perp} in models ii and iii. [b] Calculated using the modified Oseen tensor. [c] Calculated using the Oseen tensor. [d] Calculated for C^α model with the addition of a 2 Å layer of water (88 molecules), added using InsightII (Biosym Inc., San Diego, CA). Each water molecule was represented as a sphere with a 1.6 Å radius. [e] From ^{1}H PFG NMR data.

difficult to predict *a priori* the amount of water required, as this can vary substantially from one protein to another (Venable & Pastor, 1988). An experimental measurement of the translational diffusion coefficient could potentially provide the information needed to calibrate the hydrodynamic calculation.

We have tested this approach using the small, approximately spherical protein ubiquitin (the ratio of the principal moments of the inertial tensor are 1.50:1.11:1). Figure 5 illustrates the ^{1}H PFG NMR diffusion data used to measure the translational diffusion coefficient of ubiquitin [$(1.52 \pm 0.05) \times 10^{-10}$ m^2 s^{-1}], and Table 2 gives the values of D_t and of the rotational diffusion coefficients about three orthogonal axes (D_{xx}, D_{yy}, and D_{zz}) calculated using the hydrodynamic programs HYDRO (Torre, 1994) and HI4 (FORTRAN source code obtained from R. M. Venable and R. W. Pastor). It can be seen that, while the calculated translational diffusion coefficients both agree reasonably well with the experimental value, the predicted rotational diffusion coefficients differ substantially from each other. Schneider *et al.* (1992) have reported ^{15}N relaxation measurements of human ubiquitin, in which they derive a rotational correlation time of 4.1 ns (at 303 K), assuming isotropic reorientation. This corresponds to an isotropic rotational diffusion coefficient of 4.1 $\times 10^7$ s^{-1} ($\tau_c = 1/(6D_{rot})$). Repeating the hydrodynamic calculations in Table 2 at 303 K gives values of 7.9 $\times 10^7$ and 3.2 $\times 10^7$ s^{-1} using HI4 and HYDRO, respectively (again assuming isotropic tumbling). There are clearly significant differences in the way the two programs calculate rotational diffusion coefficients. Part of this difference lies in the use of the Oseen (HI4) versus modified Oseen (HYDRO) tensors for describing the nature of the hydrodynamic interaction between protein and solvent.

Table 3: Predicted Translational and Rotational Diffusion Coefficients for rJunLZ from the Hydrodynamics Programs HYDRO and HI4 Together with Experimentally Determined Values[a]

	D_t ($\times 10^{10}$ m^2 s^{-1})	D_{xx} ($\times 10^{-7}$ s^{-1})	D_{yy} ($\times 10^{-7}$ s^{-1})	D_{zz} ($\times 10^{-7}$ s^{-1})
HYDRO[b]	1.35	1.06	1.08	2.85
HI4[c]	1.62	1.46	2.00	8.73
HI4[b]	1.54	1.67	1.71	13.6
HYDRO + H_2O[b,d]	1.26	0.97	1.00	2.43
HI4 + H_2O[b,e]	1.37	1.25	1.33	4.95
D_t (obs)	1.36			

[a] All calculations were carried out using the C^α atom coordinates from the NMR solution structure of sJunLZ, so that the protein is represented as 86 spheres with 3.5 Å radii. Note that D_{zz} corresponds to D_{par}, and $D_{xx} \approx D_{yy}$ corresponds to D_{perp} in models ii and iii. [b] Calculated using the modified Oseen tensor. [c] Calculated using the Oseen tensor. [d] Calculated for C^α model with the addition of a 1.5 Å layer of water (40 molecules), added using InsightII (Biosym Inc., San Diego, CA). Each water molecule was represented as a sphere with a 1.6 Å radius. [e] Calculated for C^α model plus 40 molecules of water, as described above.

Note that in the case of ubiquitin, 88 explicitly included water molecules are necessary to reproduce the experimental translational diffusion coefficient. In comparison, previous work has shown that for the proteins hen egg white lysozyme and ribonuclease, 301 and 100 bound waters, respectively, were required in the hydrodynamic model to concur with experimental diffusion measurements (Venable & Pastor, 1988). The differences observed between proteins clearly show the potential danger in using hydrodynamic calculations to estimate rotational diffusion coefficients without having some independent data against which to calibrate the calculations. However, even with knowledge of the translational diffusion coefficient, there is clearly a dependence of the derived rotational diffusion coefficients on the mathematical model chosen to perform the calculations. In addition, while the measured and calculated values of D_t may be matched by the inclusion of bound water, the reliability of the rotational diffusion coefficients thus derived is probably dependent on the shape and rugosity of the protein−water complex.

An attempt was made to apply this method to rJunLZ; Figure 5 shows the PFG diffusion measurements and Table 3 shows the calculated hydrodynamic parameters. Reasonable agreement with the measured D_t [$(1.36 \pm 0.01) \times 10^{-10}$ m^2 s^{-1}] is obtained by HYDRO without the inclusion of any explicitly defined water molecules. However, the corresponding value of D_{perp} (1.07×10^7 m^2 s^{-1}) is significantly different from that calculated using the T_1/T_2 data above (1.56×10^7 m^2 s^{-1}). For HI4, good agreement of calculated D_t with the measured value is obtained by adding 40 water molecules, but again the corresponding rotational diffusion coefficients are very different from the T_1/T_2-derived estimates. The observation that the rotational diffusion coefficients obtained by fitting the relaxation data do not agree with those obtained from translational diffusion measure-

ments/hydrodynamic calculations is interesting. One possible cause for the discrepancy between these techniques is that protein aggregation is affecting the results. This explanation, however, is unlikely. The molecular mass estimated for rJunLZ obtained by substituting the measured value of D_t into eq 16 is 11 ± 2 kDa, which is in good agreement with the actual molecular mass of 10.6 kDa. This result suggests that non-specific aggregation is probably not significant for the rJunLZ dimer under these conditions. In any case, it is important to realize that even if measurements of the rotational diffusion constants obtained from the ^{15}N relaxation data are biased in some sense by protein aggregation, these estimates are probably still the ones which will best enable information on internal motions to be extracted from the relaxation data (although if aggregation *is* significant, the interpretation of any extracted parameters will obviously be obscured). For this reason, and because of the variability of the hydrodynamic approach based on D_t, it was decided to use the estimates of D_{par} and D_{perp} derived from the T_1/T_2 analysis for the subsequent fitting procedure.

Model-Free Analysis. Using the estimates of the rotational diffusion coefficients obtained in the preceding section, the model-free parameters S^2 and τ_e were calculated by minimization of the merit function (Stone *et al*., 1992)

$$\chi_i^2 = \left[\frac{(T_{1,i}^{obs} - T_{1,i}^{calc})^2}{\sigma_{1,i}^2} + \frac{(T_{2,i}^{obs} - T_{2,i}^{calc})^2}{\sigma_{2,i}^2} + \frac{(NOE_{1,i}^{obs} - NOE_{1,i}^{calc})^2}{\sigma_{NOE,i}^2}\right] \quad (17)$$

where P_i^{obs} is the observed value of a relaxation measurement for residue i, P_i^{calc} is the calculated value for the same parameter, and σ_i is the standard deviation in the measurement of P_i^{obs} ($P_i = T_1$, T_2, NOE). The value of χ_i^2 was minimized for each residue, giving initial estimates for τ_e and S^2. These estimates for the model-free parameters are dependent on the estimates for D_{par} and D_{perp}, which have been shown to contain a significant amount of uncertainty. Consequently the values for the diffusion constants were optimized in a grid search procedure. In this procedure an overall χ^2 value was calculated, χ_t^2, by summation of χ_i^2 over all of the residues. The values of the diffusion constants were then varied systematically in a two-dimensional grid search until the minimum value for χ_t^2 was found. A 95% confidence interval for the resulting diffusion coefficients is $D_{par} = (2.6 \pm 0.3) \times 10^7$ s^{-1} and $D_{perp} = (1.486 \pm 0.028) \times 10^7$ s^{-1}. Using these values for the diffusion coefficients, model-free parameters were extracted from the relaxation data and are displayed in Figure 6. Uncertainties in the calculated parameters were calculated by carrying out 500 Monte Carlo simulations. The Monte Carlo simulations were performed twice: the first simulation took into account only the errors in the relaxation data while the second simulation incorporated the uncertainties in both the relaxation data and the angles, α_i. It was thought that since the value of α_i has a large effect on the calculated values of T_1 and T_2, large uncertainties in α_i would lead to large uncertainties in S^2. Fortunately, in this case, the average standard deviation in S^2 increases only marginally from 0.04, when uncertainties in the angle are not accounted for, to 0.043 when the uncertainties in α_i are included in the Monte Carlo simulations.

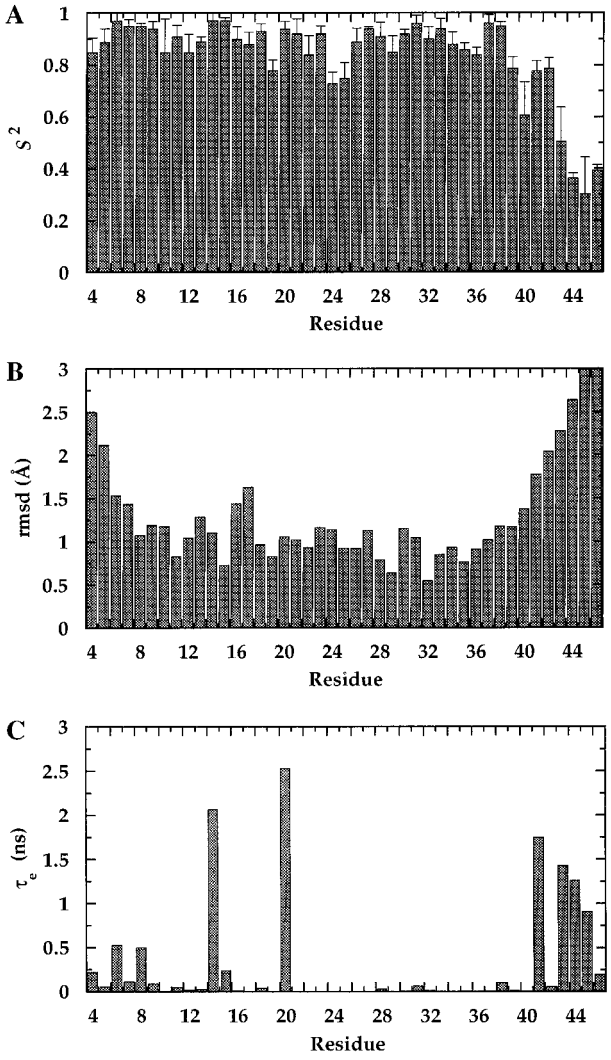

FIGURE 6: (A) Graph of the order parameter S^2 against residue number for rJunLZ. The errors shown are standard deviations and are derived from 500 Monte Carlo simulations of the data. (B) Mean backbone rmsds for individual residues for the family of seven NMR-derived solution structures of rJunLZ (Junius *et al*., 1996). Rmsds were obtained by superimposing structures pairwise onto the lowest energy structure and then averaging over the six different pairs. (C) Graph showing the internal correlation time τ_e for each residue. No quantitative conclusions may be drawn from these values; consequently, error bars are not shown.

The observation that uncertainties in α_i do not affect significantly the uncertainty in S^2 can be understood by considering what happens when α_i is decreased from its "true" value. The calculated value of T_1 will increase, and the calculated value of T_2 will decrease. It is not possible to alter S^2 in a way which will simultaneously account for both these changes since S^2 affects T_1 and T_2 in the same way (van Mierlo *et al*., 1993), and so the fitted value of S^2 will not change very much. The value of τ_e was found to be more sensitive to the uncertainty in α_i; the uncertainty in τ_e increased by 43% on average when the uncertainties in α_i were included in the Monte Carlo simulations. As observed elsewhere [see, for example, Stone *et al*. (1993)] the uncertainities in τ_e are large. This is a result of the insensitivity of χ_i^2 to the value of τ_e and makes interpretation of the τ_e data less reliable than intepretation of the order parameters. Consequently only the uncertainities in the order parameters are displayed and only these model-free parameters are intepreted in terms of internal molecular motion.

DISCUSSION

Relatively few ^{15}N relaxation studies have been reported to date on proteins which are highly asymmetric. Barbato *et al*. (1992) studied calmodulin, which appears from the crystal structure to be a rigid dumbbell shape (Babu *et al*., 1988). However, it was shown that, in solution, the protein could be adequately represented by two isotropically tumbling domains, implying that the linker region connecting the two domains is flexible; this allowed the simpler isotropic model (eq 1) to be used in the analysis of the relaxation data. Zink *et al.* (1994) and Zheng *et al.* (1995) used anisotropic models to analyze ^{15}N relaxation data recorded on human granulocyte colony-stimulating factor (rh-met-GCSF) and *trp* repressor, respectively.

The rJunLZ dimer is highly asymmetric (Junius *et al*., 1996), so a modified expression for the spectral density function (eq 2) was required to adequately interpret the ^{15}N NMR relaxation data. In this model, the value of the spectral density functions for a particular N−H unit are dependent on the angle made between the N−H vector and the principal axis of the protein, so that errors in the angles will be manifested in the final fitted parameters. Note that, although the use of a single angle for mobile residues may appear to be a contradiction, this condition is implicit in the assumption that the internal motions are much faster than the overall molecular tumbling (the angle α is by definition an angle averaged by the fast internal motions). This decoupling of overall motion from internal motion appears to constitute a reasonable approximation for isotropically tumbling proteins (Lipari & Szabo, 1982a,b) and should hold for anisotropic proteins as well.

Because nearly all of the N−H vectors in the rJunLZ dimer point in a similar direction, at a small angle to the long axis of the molecule, the rotational diffusion coefficient D_{par} may be poorly defined. Indeed, the ratio of D_{par}/D_{perp} is somewhat smaller than that predicted either from hydrodynamic calculations or from a simpler model where the protein is approximated by a prolate ellipsoid. An attempt was made to use the translational diffusion coefficient, measured using a PFG NMR experiment, to provide an independent estimate of D_{par} and D_{perp}, but it appears that the derived rotational diffusion coefficients are rather dependent on the model chosen to carry out the hydrodynamic calculations.

The calculated order parameters were consistently in the range 0.7−0.9 for all residues in the rJunLZ dimer, except for several residues at the C-terminus (Figure 6A), which shows substantially lower order parameters, as expected if the two helices constituting the coiled-coil fray at this end. This is consistent with the NMR data for rJunLZ (Junius *et al*., 1996), which reveals fewer NOEs in this region. The N-terminus is somewhat more ordered due to the disulfide bond at Cys 4. Figure 6B shows a plot of the backbone rmsds on a residue-by-residue basis for the calculated family of seven rJunLZ solution structures (Junius *et al*., 1996). This plot exhibits similar trends to the ^{15}N relaxation data. Taken together, these data are consistent with a model in which the conformational exchange process previously reported for rJunLZ is confined to the side chain of Asn22 and does not substantially affect the mobility of the peptide backbone. Figure 6C shows the derived values of the internal correlation time, τ_e, for each residue, and there appears to be a substantial variation in this parameter without a discernable trend (other than that at the C-terminus). Similar observations have been made in most studies of this type, and, typically, little significance has been placed on the values of this parameter.

It is interesting that the order-parameter profile (Figure 6A) shows no significant increase in backbone mobility in the region of the polar interfacial Asn22 residue, despite its demonstrated participation in a conformational exchange process (Junius *et al*., 1995) and its substantial destabilization of the coiled-coil dimer (Alber, 1992; Junius *et al*., 1995). Note however, that although there is no evidence for increased mobility of Asn22 on the nano- to picosecond time scale, this does not necessarily mean that this residue is not more mobile on a slower time scale. One might expect to see evidence for such slow motions as exchange contributions to T_2, although the size of a potential exchange contribution is dependent on the ^{15}N chemical shift difference between the exchanging sites, the exchange rate, and the field strength of the spin-locking field in the $T_{1\rho}$ experiment (it is worth noting that the line width of the Asn22 cross-peak in the ^{15}N dimension of HSQC spectra recorded between 273 K and 310 K was indistinguishable from those of other residues in the structured region of the protein). Thus the failure to observe an exchange contribution does not necessarily imply that slow motions do not occur. Despite this caveat, the lack of additional mobility observed for Asn22 suggests that the instability conferred by this residue may result largely from its unfavorable location at the hydrophobic dimer interface rather than being a consequence of motional disorder introduced into the helical backbone of the zipper. Thus, the conformational exchange process previously observed for this residue (Junius *et al*., 1995) is probably confined to the Asn side chains. In fact, this motional disorder might provide some entropic compensation for its enthalpically unfavorable desolvation; this information will clearly be helpful in our quest to rationally design dominant negative leucine zipper domains which can sequester native c-Jun and c-Fos in neoplastic tissue (John *et al*., 1994).

ACKNOWLEDGMENT

Dr. Bill Bubb is thanked for expert maintenance of the 600 MHz NMR spectrometer, and Dr. Peter Baron of Bruker Australia is thanked for providing time on their DRX500 NMR spectrometer. We thank Prof. Jean-François LeFèvre for valuable discussions and for raising the idea of using translational diffusion measurements to estimate rotational correlation times for the analysis of ^{15}N nuclear relaxation data. Dr. Bill Broadhurst and Dr. Martin Stone are thanked for valuable discussions. Andrew Dingley is thanked for assistance with the PFG NMR experiments.

REFERENCES

Abragam, A. (1961) *Principles of Nuclear Magnetism*, Clarendon Press, Oxford.

Alber, T. (1992) *Curr. Opin. Genet. Dev. 2*, 205−210.

Angel, P. E., & Herrlich, P. A. (1994) *The FOS and JUN Families of Transcription Factors*, CRC Press, Boca Raton, FL.

Babu, Y. S., Bugg, C. E., & Cook, W. J. (1988) *J. Mol. Biol. 204*, 191−204.

Barbato, G., Ikura, M., Kay, L. E., Pastor, R. W., & Bax, A. (1992) *Biochemistry 31*, 5269−5278.

Bartels, C., Xia, T., Billeter, M., Güntert, P., & Wüthrich, K. (1995) *J. Biomol. NMR 5*, 1−10.

Bennett, W. S., & Huber, R. (1983) *CRC Crit. Rev. Biochem. 15*, 290−384.

Boyd, J., Hommel, U., & Campbell, I. D. (1990) *Chem. Phys. Lett. 175*, 477−482.
Cantor, C. R., & Schimmel, P. R. (1980) in *Biophysical Chemistry, Part II: Techniques for the Study of Biological Structure and Function*, pp 531−590, W. H. Freeman and Company, New York.
Clore, G. M., Driscoll, P. C., Wingfield, P. T., & Gronenborn, A. M. (1990) *Biochemistry 29*, 7387−7401.
de la Torre, J. G. (1994) *Biophys. J. 67*, 530−531.
de la Torre, J. G., & Bloomfield, V. A. (1981) *Q. Rev. Biophys. 14*, 81−139.
de la Torre, J. G., & Bloomfield, V. A. (1989) in *Dynamic Properties of Macromolecular Assemblies* (Harding, S. E., & Rowe, A. J., Eds.) pp 3−31, Royal Society of Chemistry, Cambridge.
Dingley, A. J., Mackay, J. P., Chapman, B. E., Morris, M. B., Kuchel, P. W., Hambly, B. D., & King, G. F. (1995) *J. Biomol. NMR 6*, 321−328.
Fersht, A. R. (1987) *Trends Biochem. Sci. 12*, 301−304.
Gibbs, S. J., & Johnson, C. S. J. (1991) *J. Magn. Reson. 93*, 395−402.
Grzesiek, S., & Bax, A. (1993) *J. Am. Chem. Soc. 115*, 12593−12594.
Harbury, P. B., Zhang, T., Kim, P. S., & Alber, T. (1993) *Science 262*, 1401−1407.
Huntress, W. T. J. (1968) *J. Chem. Phys. 48*, 3524−3533.
Hurst, H. (1994) *Protein Profile 1*, 123−152.
Jencks, W. I. (1981) *Proc. Natl. Acad. Sci. U.S.A. 78*, 4046−4050.
John, M., Briand, J., Granger-Schnaar, M., & Schnarr, M. (1994) *J. Biol. Chem. 269*, 16247−16253.
Junius, F. K., Mackay, J. P., Bubb, W. A., Jensen, S. A., Weiss, A. S., & King, G. F. (1995) *Biochemistry 34*, 6164−6174.
Junius, F. K., O'Donoghue, S. I., Mackay, J. P., Nilges, M., Weiss, A. S., & King, G. F. (1996) *J. Biol. Chem.* (in press).
Karplus, M., & McCammon, J. A. (1983) *Annu. Rev. Biochem. 53*, 263−300.
Kay, L. E., Torchia, D. A., & Bax, A. (1989) *Biochemistry 28*, 8972−8979.
Kördel, J., Skelton, N. J., Akke, M., Palmer, A. G. I., & Chazin, W. J. (1992) *Biochemistry 31*, 4856−4866.
Kraulis, P. (1991) *J. Appl. Crystallogr. 24*, 946−950.
Kuchel, P. W., & Chapman, B. E. (1991) *J. Magn. Reson. 94*, 574−580.
Landschulz, W. H., Johnson, P. F., & McKnight, S. L. (1988) *Science 240*, 1759−1764.
Lipari, G., & Szabo, A. (1982a) *J. Am. Chem. Soc. 104*, 4559−4570.
Lipari, G., & Szabo, A. (1982b) *J. Am. Chem. Soc. 104*, 4546−4559.
Live, D. H., Davis, D. G., Agosta, W. C., & Cowburn, D. (1984) *J. Am. Chem. Soc. 106*, 1939−1941.
Lumb, K. J., & Kim, P. S. (1995) *Science 268*, 436−438.
Marion, D., & Wüthrich, K. (1983) *Biochem Biophys. Res. Commun. 113*, 967−974.
Marion, D., Ikura, M., & Bax, A. (1989) *J. Magn. Reson. 84*, 425−430.
McKnight, S. L. (1991) *Sci. Am. 264*, 32−39.
McLachlan, A. D., & Stewart, M. (1975) *J. Mol. Biol. 98*, 293−304.
Messerle, B. A., Wider, G., Otting, G., Weber, C., & Wüthrich, K. (1989) *J. Magn. Reson. 85*, 608−613.
Mierlo, C. P. M. v., Darby, N. J., Keeler, J., Neuhaus, D., & Creighton, T. E. (1993) *J. Mol. Biol. 229*.
Nirmala, N. R., & Wagner, G. (1988) *J. Am. Chem. Soc. 110*, 7557−7558.
Nirmala, N. R., & Wagner, G. (1989) *J. Magn. Reson. 82*, 659−661.
O'Shea, E. K., Klemm, J. D., Kim, P. S., & Alber, T. (1991) *Science 254*, 539−544.
Page, M. I., & Jencks, W. A. (1971) *Proc. Natl. Acad. Sci. U.S.A. 68*, 1678−1683.
Palmer, A. G., III, Cavanagh, J., Wright, P. E., & Rance, M. (1991a) *J. Magn. Reson. 93*, 151−170.
Palmer, A. G., III, Rance, M., & Wright, P. E. (1991b) *J. Am. Chem. Soc. 113*, 4371−4380.
Riley, L. G., Junius, F. K., Swanton, M. K., Vesper, N. A., Williams, N. K., King, G. F., & Weiss, A. S. (1994) *Eur. J. Biochem. 219*, 877−886.
Ringe, D., & Petsko, G. (1985) *Prog. Biophys. Mol. Biol. 45*, 197−235.
Rischel, C., Madsen, J. C., Andersen, K. V., & Poulsen, F. M. (1994) *Biochemistry 33*, 13997−14002.
Schneider, D. M., Delwo, M. J., & Wand, A. J. (1992) *Biochemistry 31*, 3645−3652.
Shaka, A. J., Barke, P. B., & Freeman, R. (1985) *J. Magn. Reson. 64*, 547−552.
Shoji, A., Ozaki, T., Fujito, T., Deguchi, K., Ando, S., & Ando, I. (1989) *Macromolecules 22*, 2860−2863.
Shoji, A., Ozaki, T., Fujito, T., Deguchi, K., Ando, S., & Ando, I. (1990) *J. Am. Chem. Soc. 112*, 4693−4697.
Skelton, N. J., Palmer, A. G., III, Akke, M., Kördel, J., Rance, M., & Chazin, W. J. (1993) *J. Magn. Reson., Ser. B 102*, 253−264.
Sørensen, M. D., Kristensen, S. M., & Led, J. J. (1995) *J. Magn. Reson. Ser. B 107*, 83−87.
Stejskal, E. O., & Tanner, J. E. (1965) *J. Chem. Phys. 42*, 288−292.
Stone, M. J., Fairbrother, W. J., Palmer, A. G., III, Reizer, J., Saier, M. H. J., & Wright, P. E. (1992) *Biochemistry 31*, 4394−4406.
Stone, M. J., Chandrasekhar, K., Holmgren, A., Wright, P. E., & Dyson, H. J. (1993) *Biochemistry 32*, 426−435.
Venable, R. M., & Pastor, R. W. (1988) *Biopolymers 27*, 1001−1014.
Waldeck, A. R., Lennon, A. J., Chapman, B. E., & Kuchel, P. W. (1993) *J. Chem. Soc., Faraday Trans. 89*, 2807−2814.
Williams, D. H., Cox, J. P. L., Doig, A. J., Gardner, M., Gerhard, U., Kaye, P. T., Lal, A. R., Nicholls, I. A., Salter, C. J., & Mitchell, R. C. (1991) *J. Am. Chem. Soc. 113*, 7020−7030.
Williams, R. J. P. (1989) *Eur. J. Biochem. 183*, 479−497.
Woessner, D. E. (1962) *J. Chem. Phys. 37*, 647−654.
Zheng, Z., Czaplicki, J., & Jardetzky, O. (1995) *Biochemistry 34*, 5212−5223.
Zhou, N. E., Kay, C. M., & Hodges, R. S. (1994) *Protein Eng. 7*, 1365−1372.
Zink, T., Ross, A., Lüers, K., Ciesler, C., Rudolph, R., & Holak, T. A. (1994) *Biochemistry 33*, 8453−8463.

BI952761Y